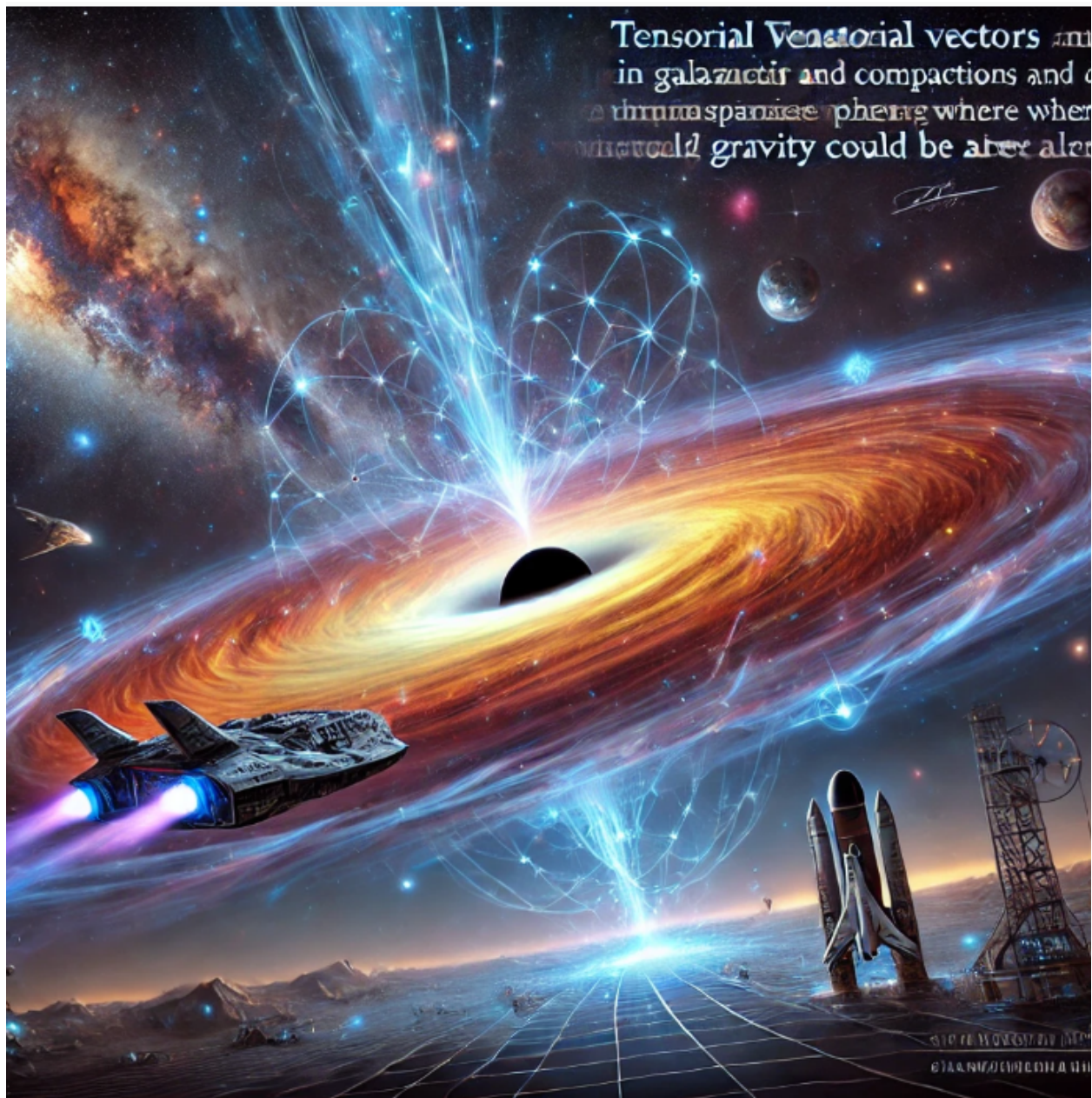


Compactified dimensions in black holes for the design of turbofan space engines and for the design of the fuselage and new physics concepts



The central axis is the dimensional structure of a turbofan and the tensor or dimensional structure of a black hole to create a new physics-engineering object. Gravitational waves are key to detecting and studying these exotic objects in extra dimensions. The Alcubierre theory. To create propulsion systems based on extreme gravitational effects (Alcubierre type), we could explore:

1. Generation of artificial gravitational structures (massive binaries, matter accumulation, dark energy manipulation).
2. Use of gravitational waves to induce impulses or locally distort space.
3. Application of theories of extra dimensions to find new forms of gravitational control.
4. Interaction with quantum black holes or negative energy structures to achieve controlled space-time curvatures. "exploring ways to combine the pieces of a black hole with additional components and dimensions that could be incorporated into a spacecraft engine or turbo propulsor. This also includes the theoretical possibility of gravitational manipulation with this new space object, incorporating Alcubierre drive and CTS (Curvature-Twisted Space).

1. Creation of new stars or massive gravitational structures

In theory, certain astrophysical processes can give rise to new massive objects that could serve as sources of gravitational energy or space-time distortion:

Neutron star collision: Can generate a higher mass star or even collapse into a black hole. It can also release enormous amounts of energy in the form of gravitational waves.

Gas accretion in molecular clouds: In dense regions of space, the accretion of matter could create massive new stars.

Dark matter and exotic gravitational structures: If dark matter or dark energy could be manipulated, massive structures could be formed without the need for ordinary matter.

2. Propulsion based on space-time distortions (Alcubierre Engine and variants)

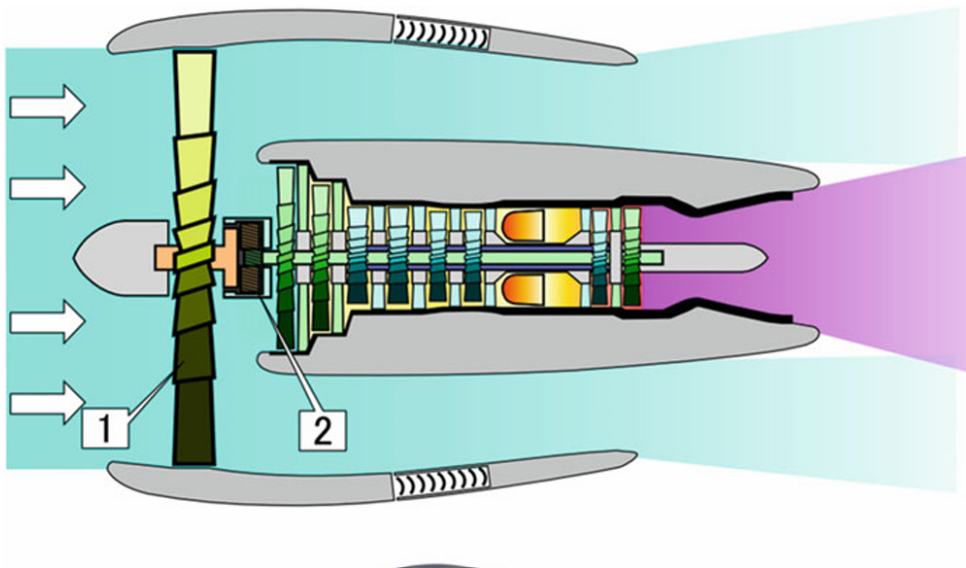
The Alcubierre engine is a theoretical solution to general relativity that would allow faster-than-light travel without violating causality. Its operation is based on:

Expansion and contraction of space-time: A negative energy would be needed (possibly quantum vacuum energy or exotic effects from extra dimensions).

Extreme mass/energy to induce curvature: If we could generate intense but controlled gravitational structures, they could be used to manipulate the space-time fabric.

Possible ways to create these effects:

1. Use of microscopic black holes as a source of localized gravitational distortion.
2. Manipulation of exotic matter with negative energy density (string theories, Casimir, quantum effects).
3. Use of gravitational waves at certain frequencies to induce fluctuations in space-time.



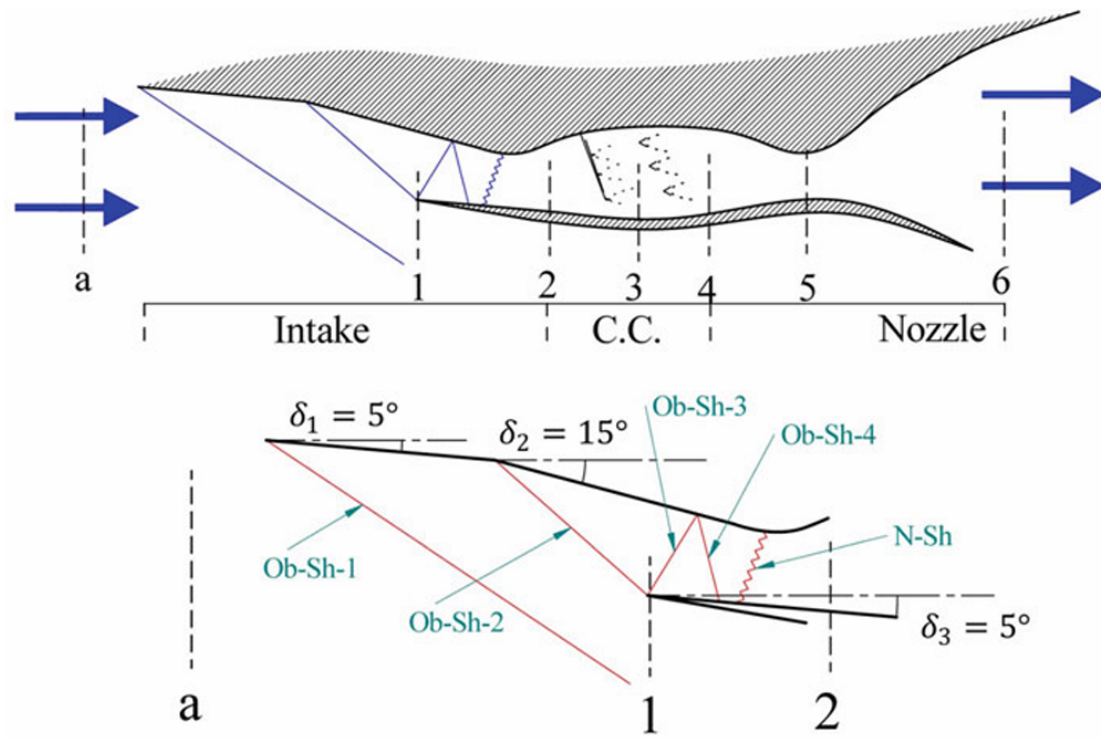
3. Extreme binary systems and their possible application in propulsion

A rapidly rotating binary system of black holes or neutron stars generates powerful gravitational waves. If we could extract energy from these waves, we could obtain a form of propulsion:

Collision chain reaction: If pairs of black holes or neutron stars were manipulated, fusions could be induced that would release usable energy.

Energy extraction from ergospheres: In rotating black holes (Kerr), the rotation energy could be used with relativistic effects (Penrose mechanism).

Propulsion using directed gravitational waves: In theory, if the emission of gravitational waves could be modulated, usable thrust could be generated.

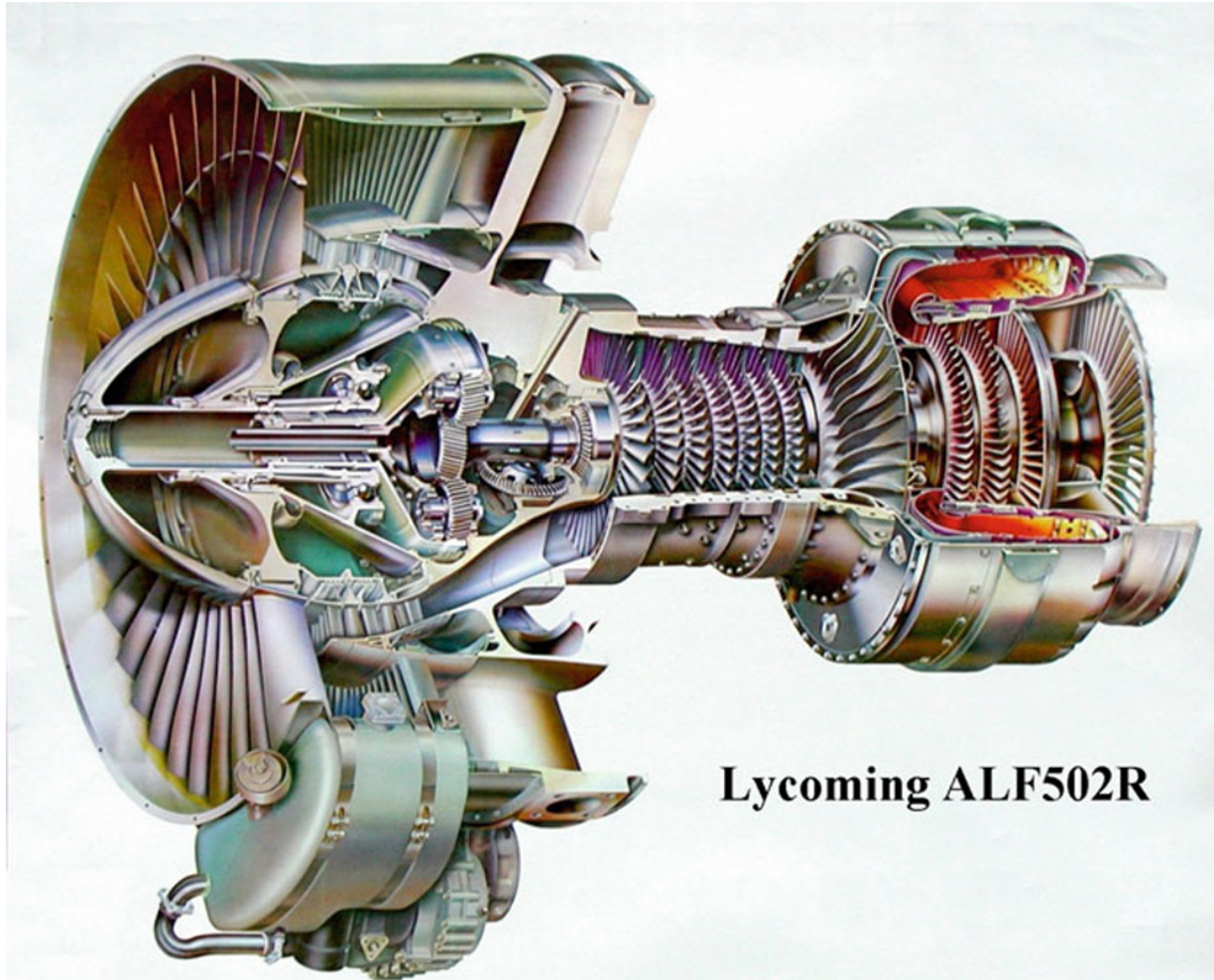


Spacetime is called spherically symmetric if there exist coordinates in which its metric takes the form $ds^2 = \gamma AB dx^A dx^B + r^2 d\omega^2$, (6.1.1) where $\gamma AB = \gamma AB(x)$, $r = r(x)$ ($A, B = 0, 1$), and $d\omega^2$ is a metric on a unit 2-dimensional sphere S^2 . $d\omega^2 = \omega_{XY} d\zeta_X d\zeta_Y$. This metric admits 3 Killing vectors $\xi_1 = -\cos\theta \partial_\phi + \cot\theta \sin\theta \partial_\theta$, $\xi_2 = \sin\theta \partial_\theta + \cos\theta \partial_\phi$, $\xi_3 = \partial_\phi$. Problem 6.1: Prove that the commutators of these vector fields are of the form where ijk is a 3D Levi-Civita symbol.

$[\xi_i, \xi_j] = ijk \xi_k$, (6.1.2) (6.1.3) (6.1.4) In the flat spacetime the vectors ξ_i are the generators of the rotation group, that is usual operators L_X , L_Y and L_Z of the angular momentum. Under the action of the symmetry transformations a point remains on a surface of constant radius r . Any two points on this 2D surface can be obtained from one another by the action of the symmetry transformation. Besides the continuous isometries generated by the Killing vectors, the metric The discrete symmetries: $\phi \rightarrow -\phi$, $\theta \rightarrow \pi - \theta$.

under all the isometries of a two-sphere. Prove that $a = \text{const}$, $a_X = 0$, $a_X Y = \text{const}$ $\delta X Y$. (6.1.6) In a spherically symmetric spacetime a tensor $Q_{\mu\nu}$ that obeys this symmetry satisfies the conditions $L\xi_i Q_{\mu\nu} = 0$, $i = 1, 2, 3$.

the Einstein tensor $G_{\mu\nu}$. The conservation law $G_{\mu\nu;\mu} = 0$, implies $G_{AB;A} + 2r_A r_B G_{AB} - 2r_B r_A G_{AB} = 0$



thermodynamic analysis of geared turbofan, if the mechanical efficiency of the gearbox is η_{gb} , then two cases are examined. Firstly, the low-pressure spool is composed of a fan and a low-pressure turbine. The fan states are 2 and 3 and the LPT states are 6 and 7. Then energy balance is expressed by the relation: $1/\rho \dot{m}_a C_p (T_{03} - T_{02}) = \eta_{gb} (\dot{m}_b C_p (T_{06} - T_{07}) - \dot{m}_a C_p (T_{06} - T_{07}))$. \dot{m}_a is the air bleed ratio defining the ratio between the air bled and the HPC to the core airflow rate. transformation laws, and operations like symmetrization, antisymmetrization, and contraction. Tensors are mathematical objects that transform according to specific rules under a change of coordinates. A tensor of rank (k, l) has components $T^{\mu_1 \dots \mu_k \nu_1 \dots \nu_l}$, and these components transform in a particular way between different coordinate systems.

The rank of a tensor (k, l) describes its number of covariant (lower indices) and contravariant (upper indices) components. Common operations on tensors include:

- Symmetrization and Antisymmetrization:** These operations modify tensors by permuting their indices, with signs depending on the permutation's parity.
- Contraction:** This operation reduces the rank of a tensor by contracting (summing over) indices.

3. **Linear Transformation of Tensors:** A tensor transforms linearly under a change of basis in its vector space.

The document also includes mathematical tools like the **Kronecker delta** and the **Young tableau**, which classify tensors based on their symmetries and help calculate their dimensions. The process of symmetrization and antisymmetrization, as well as contraction, plays an essential role in defining irreducible components of tensors.

The idea is to create metrics or black hole metrics across new materials or new objects in spaceship motors to imitate the states in the galaxy and create new models.

Dimensional reduction of the action In order to study the spherically symmetric spacetimes it is sufficient to substitute the metric ansatz Eq. (6.1.1) into the Einstein equations. But there exists an alternative way. Namely, one can substitute the ansatz Eq. (6.1.1) into the Einstein–Hilbert action Eq. (5.1.6). Since neither R nor depends on the angular variables, one can integrate over them. As a result, the Einstein–Hilbert action reduces to the action S_{sp} , which is a function of the two dimensional metric γ^{AB} and the scalar field r , $S_{\text{sp}} = S_{\text{sp}}[\gamma, r]$. Both of these field variables depend only on the x^A coordinates, so that the original 4D problem is reduced to the 2D one.

Propulsion structure-across black hole pieces

Turbofan-black hole design: $\delta \mathbf{P} _ \text{maCpc T010 T02} \delta \mathbf{p} _ {}^{1/4} \eta g b \lambda l \eta m 1 _ \text{ma 1} \mathbf{p} \ f \mathbf{b} \ \text{mCpc T03 T010} \delta \mathbf{p} \ \delta \mathbf{p} \text{Cph T06 T07} \delta \mathbf{p}$

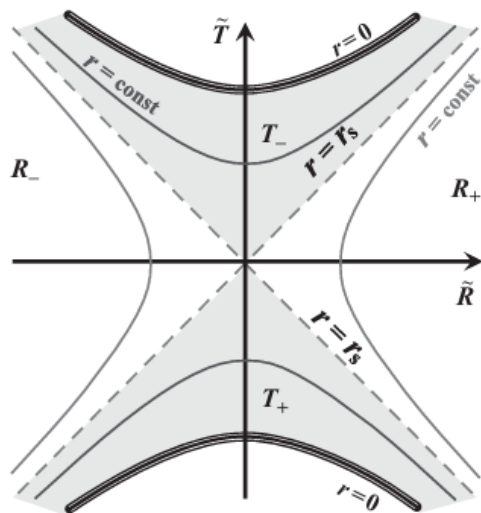


Fig. 6.2 Spherically symmetric vacuum spacetime in Kruskal coordinates.

Concerning the high-pressure spool, with an air bled from a station just downstream of HPC and prior of combustion chamber: $\text{maCpc T04 T03} \rightarrow \text{P}^{1/4}\lambda^2\eta m^2 \text{ ma 1pf b} \rightarrow \text{Pcph T05 T06}$

Forward Fan Unmixed Three-Spool Engine The three-spool engine is composed of a low-pressure, intermediate-pressure, and high-pressure spools running at different speeds (N_1 , N_2 , and N_3). The fan and the low-pressure turbine (LPT) compose the low-pressure spool. The intermediate spool is composed of an intermediate-pressure compressor (IPC) and intermediate-pressure turbine (IPT). The high-pressure spool is also composed of a high-pressure compressor (HPC) and high-pressure turbine (HPT).

The Kruskal metric Eq. (6.3.14) is invariant under the following discrete symmetries $I : U \rightarrow -U$, $T : U \rightarrow -V$, $P : U \rightarrow V$, $V \rightarrow -V$, $V \rightarrow -U$, $V \rightarrow U$.

1. Shorter modules and shafts which result in a shortened engine (a) Single-stage fan with no booster stages (b) Fewer overall compressor stages and fewer variable stages (c) Shorter high-pressure compressor
 2. Higher efficiencies as each spool is running at its “optimum speed”
 3. Greater engine rigidity
 4. Lighter weight
- The main drawbacks of thi

The global structure of the Kruskal spacetime is illustrated in Figure 6.2. Each point of this diagram is a 2D sphere. I is a reflection with respect to the point $U = V = 0$. It maps $R+ \leftrightarrow R-$ and $T+ \leftrightarrow T-$

$dU = 0$, $dV \geq 0$, Global Structure of the Schwarzschild Spacetime 175 and $dV = 0$, $dU \geq 0$. (6.3.19) Any radial future-directed time-like or null vector lies either inside the local null cone Eq. (6.3.19) or on its boundary. There is a special modification of the spacetime diagrams, similar to the Kruskal one, which makes the global causal structure of the spacetime, including its properties at infinity, more profound. Let us denote $U = \arctan U$, $V = \arctan V$. (6.3.20) This coordinate transformation brings ‘infinities’ $U = \pm\infty$ and $V = \pm\infty$ to the finite values in the coordinates space. Since for constant values of U and V the new coordinates are again constant, they are also null. The local null cones in the new coordinates are again given by straight lines at the angle $\pm\pi/4$ with respect to a horizontal line. The Kruskal diagram in the coordinates (U, V) is shown in Figure 6.3. Such spacetime diagrams where infinit

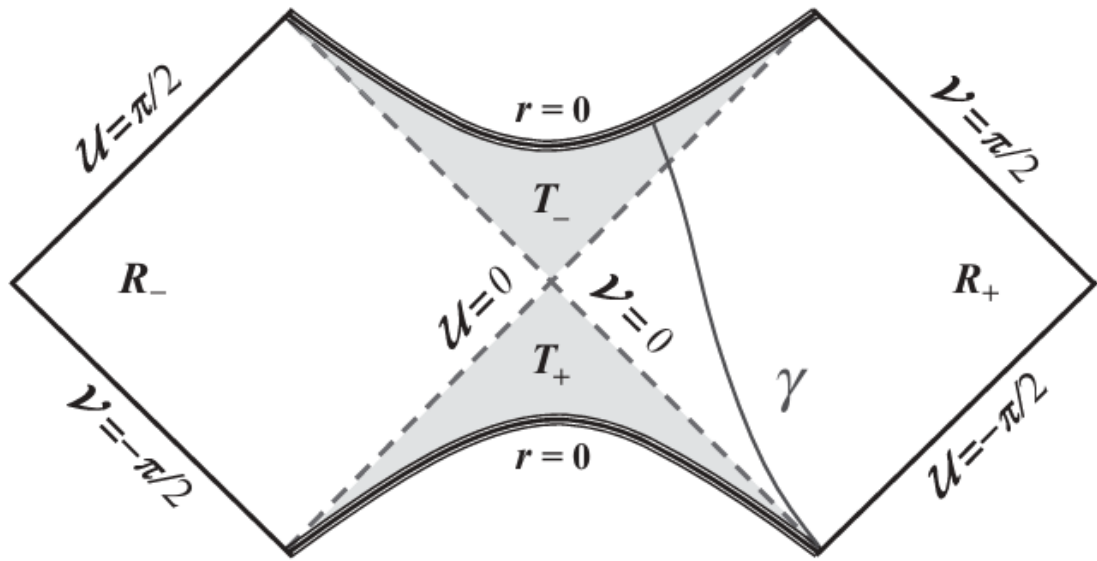


Fig. 6.3 Carter–Penrose diagram for the vacuum spacetime.

Spherically Symmetric Spacetime and Its Properties

A spacetime is called **spherically symmetric** if there exist coordinates where its metric takes the form:

$$ds^2 = \gamma_{AB} dx^A dx^B + r^2 d\omega^2, \quad (6.1.1)$$

where $\gamma_{AB} = \gamma_{AB}(x)$, $\gamma_{AB} = \gamma_{AB}(x)$, $r = r(x)$, $r = r(x)$ (with indices $A, B = 0, 1, A, B = 0, 1$), and $d\omega^2 d\omega^2$ represents the metric on the unit 2-dimensional sphere $S^2 S^2$:

$$d\omega^2 = d\theta^2 + \sin^2\theta d\phi^2, \quad d\omega^2 = d\theta^2 + \sin^2\theta d\phi^2.$$

This metric admits **three Killing vectors**:

$$\begin{aligned} \xi_1 &= -\cos\phi \partial_\theta + \cot\theta \sin\phi \partial_\phi, & \xi_1 &= -\cos\phi \partial_\theta + \cot\theta \sin\phi \partial_\phi, \\ \xi_1 &= -\cos\phi \partial_\theta + \cot\theta \sin\phi \partial_\phi, & \xi_2 &= \sin\phi \partial_\theta + \cot\theta \cos\phi \partial_\phi, \\ \xi_2 &= \sin\phi \partial_\theta + \cot\theta \cos\phi \partial_\phi, & \xi_2 &= \sin\phi \partial_\theta + \cot\theta \cos\phi \partial_\phi, \\ \xi_3 &= \partial_\phi, & \xi_3 &= \partial_\phi. \end{aligned}$$

Problem 6.1: Prove that the commutators of these vector fields take the form of the 3D Levi-Civita symbol:

$$[\xi_i, \xi_j] = \epsilon_{ijk} \xi_k, \quad (6.1.2) \quad [\xi_i, \xi_j] = \epsilon_{ijk} \xi_k, \quad \text{quad } (6.1.2) \quad [\xi_i, \xi_j] = \epsilon_{ijk} \xi_k. \quad (6.1.2)$$

In flat spacetime, the vectors $\xi^i \partial_{x^i}$ correspond to the generators of the **rotation group**, analogous to the usual angular momentum operators L_x, L_y, L_z . Under the action of these symmetry transformations, any point on the surface of constant radius r remains on that surface, meaning the transformation can move any two points on the 2D surface by the symmetry operations. This surface is termed a **transitivity surface** of the symmetry group.

Besides the continuous symmetries associated with the Killing vectors, the metric (6.1.1) has discrete symmetries:

$$\phi \rightarrow -\phi, \theta \rightarrow \pi - \theta. \quad \text{phi} \rightarrow -\phi, \theta \rightarrow \pi - \theta.$$

Thermodynamics of Turbofan Engines:

When analyzing the **mechanical efficiency of a turbofan engine**, consider the gearbox efficiency η_{gb} . For simplicity, two cases are analyzed:

1. The **low-pressure spool** consists of the fan and the low-pressure turbine (LPT). Energy balance is expressed as:

$$(1+\beta)m_a C_p (T_{03} - T_{02}) = \eta_{gb}[m_b(\lambda_1 \eta_{m1})m_a(1+f_b)C_p(T_{06} - T_{07})], \quad (1 + \beta) \dot{m}_a C_p (T_{03} - T_{02}) = \eta_{gb}[m_b(\lambda_1 \eta_{m1}) \dot{m}_a(1 + f_b)C_p (T_{06} - T_{07})],$$

where $m_a \dot{m}_a$ represents the air bleed ratio, defining the ratio of air bled from the high-pressure compressor (HPC) to the core airflow rate.

Drawing a Comparison: Turbofan Engines and Black Holes

At a conceptual level, both **turbofan engines** and **black holes** are systems that involve intricate **energy transfer and conversion** processes, yet they operate under vastly different physical principles. However, when comparing their **thermodynamic properties** and **efficiencies**, interesting parallels arise:

1. Energy Conversion Efficiency:

- In a **turbofan engine**, the goal is to convert **thermal energy** from combustion into kinetic energy efficiently, with an emphasis on reducing energy losses due to friction, heat transfer, and mechanical inefficiencies.
- In the context of a **black hole**, the efficiency could be considered in terms of its **gravitational energy** and the conversion of matter into **Hawking radiation** or the energy

released through **accretion**.

2. Symmetry and Structure:

- Both systems exhibit highly structured, symmetric properties. A **turbofan engine** has spools and turbines arranged symmetrically to optimize the energy extraction at each stage. Similarly, a **black hole's spacetime** exhibits spherical symmetry, with the **event horizon** acting as a boundary that defines the limits of the gravitational influence.

3. Role of Spacetime:

- The geometry of spacetime around a **black hole** can be described by the **Kruskal coordinates**, which help visualize the global structure of the black hole's event horizon. This is similar to understanding the **spatial dimensions** in a turbofan engine, where the geometry of airflow and turbine blades must be optimized for maximum efficiency.

4. Dimensional Reduction:

- Just as **spatial dimensions in black hole spacetimes** are reduced when applying **Kruskal diagrams** or performing dimensional reduction in Einstein's equations, we can think of reducing the system in a **turbofan engine** by examining a specific spool's performance independently of the entire engine.

Designing a Turbofan-Black Hole Hybrid:

In the context of **space propulsion systems**, the analogy extends further with the concept of designing a **turbofan-black hole hybrid engine**. Imagine an engine where the energy conversion process mimics the thermodynamic flow around a **black hole's event horizon**, using material properties that emulate the behavior of spacetime near the singularity.

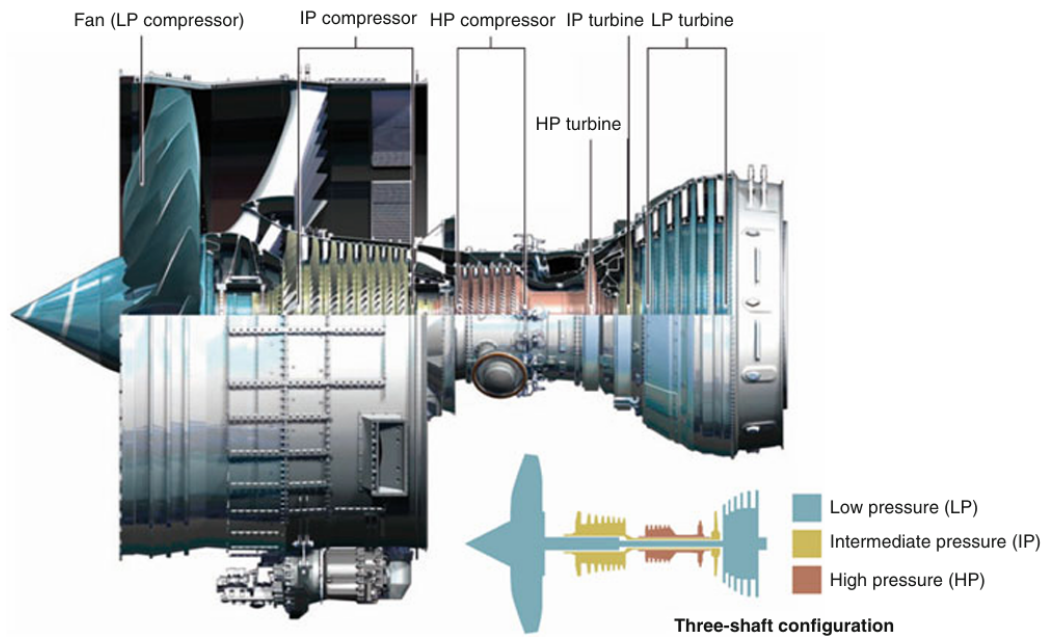
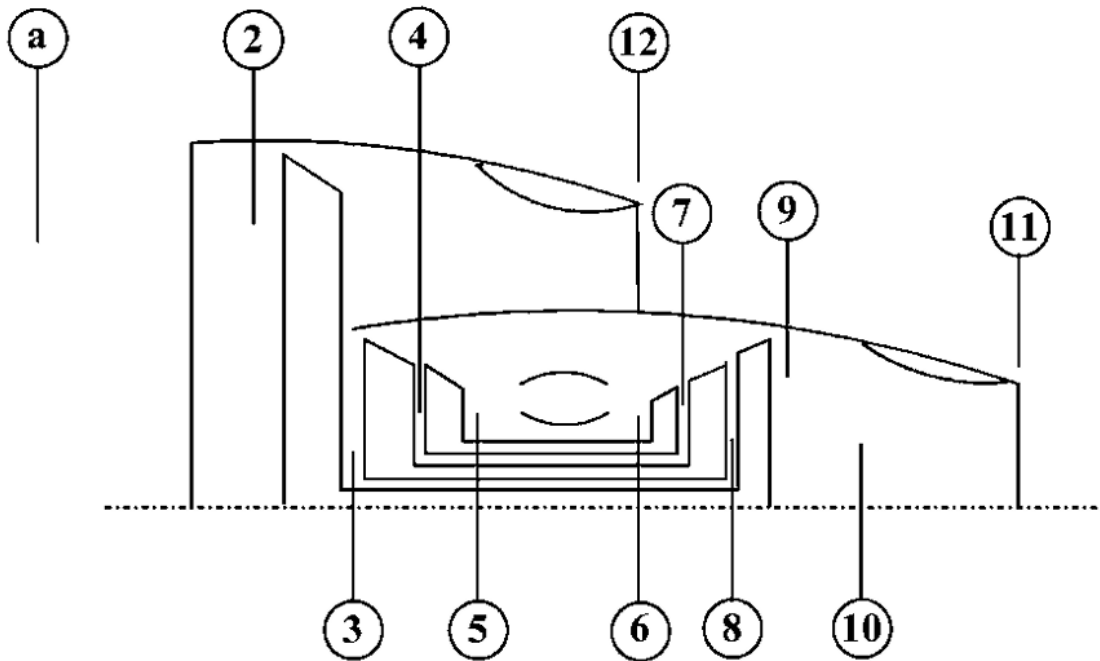


Fig. 6.26 Layout of unmixed three-spool engine (Trent 700)

6.3 Turbofan



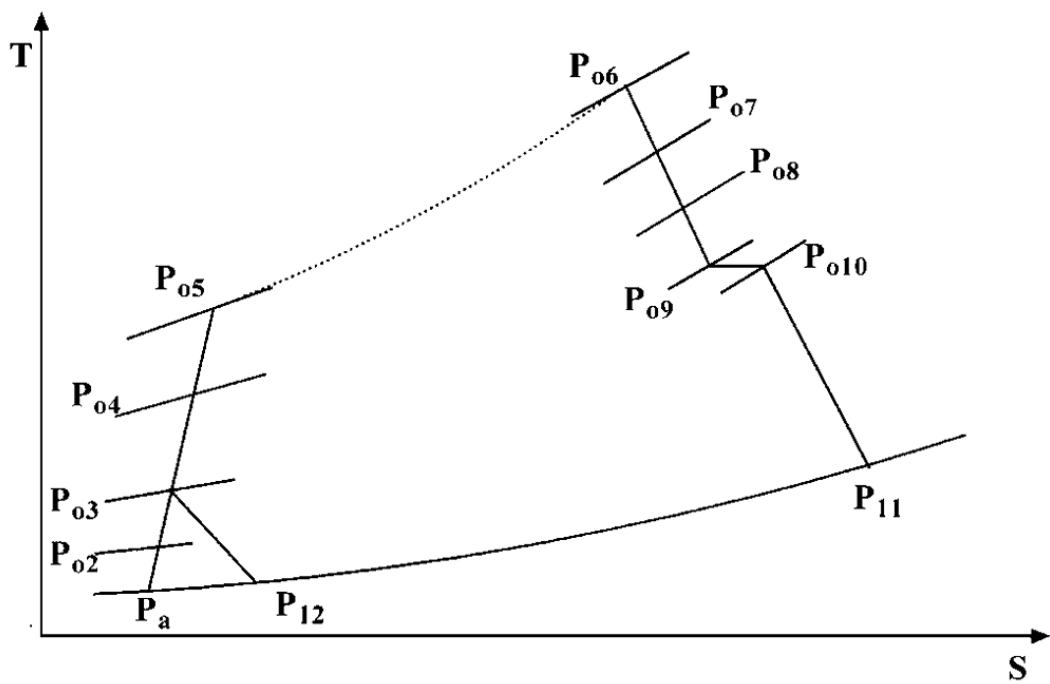


Fig. 6.25 T-s diagram for a three-spool turbofan



Besides the black hole interior (T^-) and the exterior (R^+), it contains the region T^+ , called a white hole, and R^- . The physical meaning of these regions can be clarified by analyzing concrete models of the matter source, which generates the spherically symmetric solution. For example, consider a static spherically symmetric star of radius $r_0 > r_S$, and suppose that at some moment of time $t = 0$, it loses its stability and shrinks. As a result of gravitational collapse, its surface radius decreases and crosses the Schwarzschild radius. Further evolution of the star is an inevitable continuous contraction until the curvature becomes infinitely large and a singularity is formed. The vacuum metric is valid only outside the surface of the collapsing body. This surface is represented on the Kruskal diagram (see Figure 6.3) by a time-like curve γ . Before $t = 0$, this line coincides with $r = r_0$, while for $t > 0$, γ enters the T^- region and reaches the singularity. The Kruskal diagram must be cut along this line, and the Kruskal metric is valid only in the external region located to the right of the curve γ . To determine the complete metric, one needs to solve the Einstein equations inside the matter (to the left of γ) and glue this solution with the Kruskal metric along the line γ . As a result of this procedure, the regions T^+ and R^- do not appear in the complete solution. It is clear that one may also consider matter, e.g., a dust ball, which begins its expansion in the T^+ domain, crosses the Schwarzschild surface, reaches the maximal expansion in R^+ , and then contracts until it enters the T^- region and collapses to the singularity. In order to stitch this solution to the Kruskal metric, one uses parts of the domains T^\pm and R^\pm .

Fig. 6.27 Layout of three-spool engine and air bleed details

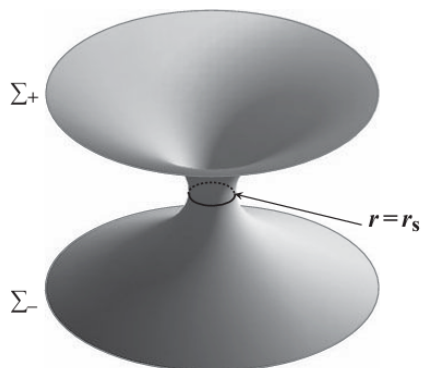
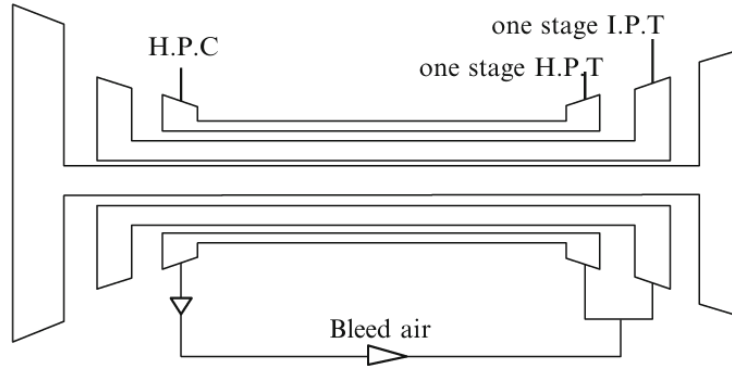
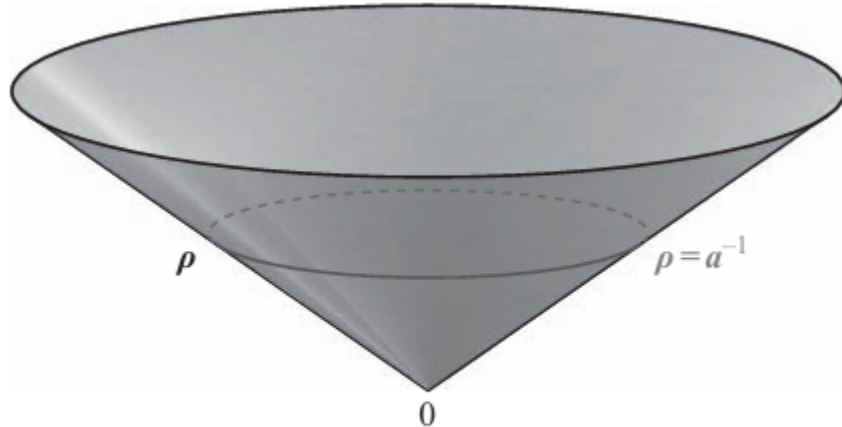


Fig. 6.4 The embedding diagram for the *Einstein-Rosen bridge*.

$$\Omega = 1 + \frac{M}{2\rho}, \quad dl_0^2 = d\rho^2 + \rho^2(d\theta^2 + \sin^2 \theta d\phi^2). \quad (6.3.30)$$

Properties- Table 6.4 A triple-spool unmixed turbofan engine operating conditions (Trent 700) Variable Value Variable η_d 0.88 Value $\Delta p_{c.c.}$ η_f 0.9 0.03 $\Delta p_{fanduct}$ η_c 0.89 0 cpc(J/kg.K) η_b 0.98 1005 cph(J/kg.K) η_t 0.93 1148 R (J/kg.K) η_n 0.98 287 γ_c η_m 0.99 1.4 γ_h λ_1 0.84 1.33 B λ_2 1 0.08 β λ_3 1 5.05 TIT(K) M π_F 0.82 π_{IPC} 1543 5.8 1.45 π_{HPC} 4.2



3. The pressure and temperature at the outlet of cold and hot nozzles 4. Specific thrust, thrust specific fuel consumption, and propulsive, thermal, and overall efficiencies. Black hole motor equation: $G(1)\beta(t,x;t,x) = -2iGF\beta(t,x;t,x) = 2GE(-it,x;-it,x)$. (9.8.24) This relation gives us the recipe for the calculation of the thermal averages using the Euclidean Green function. The renormalized Green functions are related in exactly the same way.

For a static detector in the thermal bath, the calculations show that the probability of the transition between the detector levels, in the lowest approximation in λ , is proportional to the proper time τ . The probability of the transition between levels 1 and 2 per unit time can be written in the form:

$$w^1 \rightarrow 2 = \lambda^2 Q(1,2) F(|\omega_1 - \omega_2|) G \sim \beta(\omega_2 - \omega_1). (9.8.32) \dot{w}^1 \rightarrow 2 = \lambda^2 Q(1,2)$$

Here, $\lambda^2 Q(1,2) \lambda^2 Q(1,2)$ is the "cross-section" of the interaction of the detector with the field $\phi \varphi$. Besides the coupling constant $\lambda \lambda$, it depends on the structure of the detector, which is determined by the form of the detector action and the type of interaction described by $SintS_{\text{int}}$. The factor $F(|\omega|)F(|\omega|)F(|\omega|)$ is a phase space factor, which is proportional to the density of the number of states of the quanta with frequency $(\omega, \omega + d\omega)$ ($\omega, \omega + d\omega$) in the vicinity of the detector. For the detector in the thermal bath, $G \sim \beta(\omega_2 - \omega_1) \tilde{G}(\omega_2 - \omega_1) G \sim \beta(\omega_2 - \omega_1)$ is the Fourier transform of the Matsubara function for an oscillator of frequency $\omega \omega$ in the thermal bath with inverse temperature $\beta \beta$:

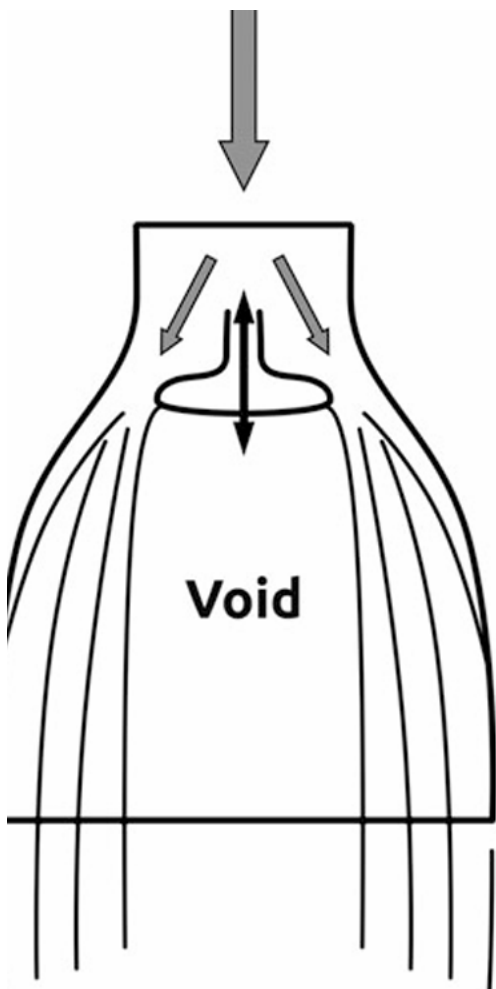
$$G \sim \beta(\omega) = \omega^2 \pi^2 e^{-\beta\omega} - 1, G \sim \beta(-\omega) = \omega^2 \pi^2 e^{-\beta\omega} - 1. \quad (9.8.33)$$

$$\tilde{G} \sim \beta(\omega) = \frac{\omega}{2\pi} e^{-\beta\omega}, \quad \tilde{G} \sim \beta(-\omega) = \frac{\omega}{2\pi} e^{-\beta\omega}. \quad (9.8.33)$$

Note that only this factor depends on the sign of the frequency ω/ω_0 , while the other factors in Eq.

(9.8.32) depend only on the absolute value $|\omega|/\omega_0$. This is why the ratio $w'_{1 \rightarrow 2}/w'_{2 \rightarrow 1} \rightarrow 1$ is universal. As a result, one has (c.s. Eq. F.3.78):

Probability of $1 \rightarrow 2$ transition per unit time \rightarrow Probability of $2 \rightarrow 1$ transition per unit time $= e^{-\beta\omega}$. $\frac{\text{Probability of } 1 \rightarrow 2}{\text{Probability of } 2 \rightarrow 1} = e^{-\beta\omega}$. Probability of $2 \rightarrow 1$ transition per unit time \rightarrow Probability of $1 \rightarrow 2$ transition per unit time $= e^{-\beta\omega}$.



1. The thrust specific fuel consumption versus Mach number ($M/40.0-0.9$)
2. The specific thrust versus Mach number ($M/40.0-0.9$)
3. The propulsive efficiency versus Mach number ($M/40.0-0.9$)
4. The

thermal efficiency versus the Mach number ($M^1/4$ 0.0–0.9) 5. The thrust specific fuel consumption versus altitude (1.0–11.0 km) for a Mach number ($M^1/4$ 0.5) 6. The specific thrust versus altitude (1.0–11.0 km) for a Mach number ($M^1/4$ 0.5) 7. The propulsive efficiency versus altitude (1.0–11.0 km) for a Mach number ($M^1/4$ 0.5) 8. The thermal efficiency versus altitude (1.0–11.0 km) for a Mach number ($M^1/4$ 0.5)

The concept of Rindler particles and the thermal properties of the Minkowski vacuum arise only when describing the corresponding processes (such as the behavior of an accelerated detector) in a uniformly accelerated frame. However, it is always possible to "return" to the inertial observer's point of view and perform the required calculations in the inertial frame. If one addresses effects that have a covariant description, the results of the calculations do not depend on the choice of the frame used for the calculations.

For example, the distribution of a uniformly accelerated detector over its internal states can be easily calculated in the Minkowski frame. However, the concept of a thermal bath of Rindler particles allows one to make quite general predictions about the properties of accelerated systems with internal degrees of freedom. This is a consequence of the universality of the thermal properties of the Minkowski vacuum in an accelerated frame.

Another aspect of the Unruh effect is a better understanding of quantum effects near the black hole horizon, in the regime where curvature effects are not important and the Rindler approximation can be used.

In higher-order dimensions and black hole physics, the Unruh effect, which describes the temperature experienced by an accelerating observer, can be explored in the context of various accelerations. For example, on the surface of the Earth, where the acceleration is 982 cm/s^2 , the resulting Unruh temperature is extremely low, around $3.98 \times 10^{-20} \text{ K}$, which is too small to be detected by current experimental setups. The thermal photon frequency in this case is also very low, about one per year.

In contrast, in systems such as linear accelerators, much higher accelerations can be achieved. At places like the Stanford Linear Accelerator, where electrons experience an acceleration of approximately $2 \times 10^{20} \text{ cm/s}^2$, the corresponding Unruh temperature is about $7 \times 10^{-3} \text{ K}$. However, in these linear accelerator experiments, there isn't enough time for the electron system to reach thermal equilibrium, as the time required for polarization to relax to equilibrium is much larger than the duration of the experiment.

Circular accelerators and storage rings offer more promising cases. For instance, in existing storage rings, electrons can achieve accelerations of about $3 \times 10^{25} \text{ cm/s}^2$. If the acceleration direction were constant, the Unruh temperature would reach around 1200 K. In this case, electrons with spins aligned with or opposite the external magnetic field have different energies, and thermal effects would lead to partial depolarization of the electron spins, a measurable effect. The polarization equilibrium could be reached within hours or even minutes.

However, in the case of circular accelerators, the direction of acceleration rotates, making a direct comparison with the Unruh effect difficult. Still, quantum calculations similar to those used in the Unruh effect could be performed, revealing similar terms in the excitation probability of the detector. In this

scenario, although the spacetime appears stationary in the reference frame of the electrons, the vacuum is no longer purely thermal, contrary to what happens in the linear acceleration case. Nonetheless, spontaneous excitation of the stationary detector is still present, and the excitation probability would be of the same order as that of the detector in a thermal bath at the Unruh temperature.

For instance, in a constant magnetic field, the spin of electrons interacts with the field, leading to spontaneous spin flips and photon radiation, as predicted by quantum calculations. This results in a polarization mixture of up- and down-polarized electrons, rather than a 100% polarization. In ideal conditions, such as those in electron storage rings, the polarization can reach around 92%, a phenomenon known as the Sokolov–Ternov effect, which has been observed in real accelerators.

Proton accelerators, such as those in the Large Hadron Collider (LHC), are less efficient in this regard because protons are more massive than electrons, leading to smaller accelerations and much longer relaxation times. The LHC, with a radius of 4.3 km and a projected proton energy of 7 TeV, experiences accelerations that can be estimated from the formula $a = (\gamma^2 - 1)c^2/R$, where γ is the Lorentz factor.

In the case of the **F-111A fighter aircraft** flying at an altitude of **13,700 meters**, with ambient conditions of **14,794 Pa** pressure and **216.66 K** temperature, we can extend the analogy of acceleration effects to understand how high accelerations experienced by objects in extreme environments—whether in near-black hole regions or within the context of advanced aviation—relate to the Unruh temperature and the associated quantum effects.

1. **Acceleration and Unruh Temperature in Aviation:** The F-111A, powered by **two Pratt & Whitney TF30 afterburning turbofan engines**, experiences a significant amount of acceleration as it maneuvers through the atmosphere. If we analyze the **acceleration of the aircraft** in relation to the Unruh effect, it is important to understand that the acceleration experienced by the aircraft would generate a very small Unruh temperature in the local frame. However, the acceleration is still small compared to those found in particle accelerators or black hole regions, meaning the thermal effects would be negligible for practical detection in this scenario.
2. **Comparing the F-111A to a Black Hole's Horizon:** Black holes, with their immense gravitational acceleration at the event horizon, create an extreme analogy to the forces experienced in a high-speed aircraft. In both scenarios, **acceleration** plays a pivotal role in how observers perceive temperature and vacuum fluctuations. For the aircraft, although the Unruh temperature from its acceleration would be exceedingly small (far smaller than the temperature of the Earth's surface), it highlights the broader principle that accelerated frames—whether on Earth or near a black hole—experience unique physical effects, such as the appearance of thermal radiation (Unruh radiation) from a vacuum that appears empty to an inertial observer.

In the black hole case, near the event horizon, the **Rindler particles** (or thermal radiation) are predicted to appear due to the intense acceleration, which in turn makes the vacuum look "hot" to an observer inside the accelerated frame. This concept is crucial when discussing the behavior of **accelerated detectors** in such environments, where the proper time experienced by the detector leads to observable thermal effects, like the **Unruh temperature**. This is analogous to how **thermal fluctuations** would be present in a black hole's frame, and in the case of the aircraft, the

local acceleration causes negligible effects but still follows the same theoretical framework.

3. **Combining Acceleration with Black Hole Physics:** In a **black hole's frame**, the **spacetime curvature** near the event horizon affects the motion of particles in a way that is mathematically similar to the acceleration of the aircraft. In both cases, objects experience accelerated motion, but the key difference lies in the magnitude of acceleration. The acceleration in the vicinity of a **black hole** creates conditions under which the thermal radiation is more pronounced, and this thermal radiation can be related to the **Rindler particles** discussed earlier.
4. **Spacetime in Circular Accelerators vs. Black Hole Frames:** Just as **circular accelerators** can generate extreme accelerations and produce measurable effects like **spin flips** (as in the **Sokolov–Ternov effect**) in electron storage rings, **highly curved spacetime near black holes** can lead to similar quantum effects. In both environments, while the detector or observer experiences accelerated motion, the surrounding vacuum doesn't appear purely thermal in an inertial frame. Instead, **spontaneous excitation** occurs, whether in a particle accelerator or near a black hole, producing observable effects such as **depolarization** in electron spins, which can be seen as a direct consequence of the quantum effects resulting from acceleration.
5. **Black Hole Acceleration and Quantum Effects:** Much like the **proton accelerators** (e.g., **LHC**), the intense **gravitational acceleration near a black hole** significantly alters the spacetime curvature. In this regime, quantum effects, such as the emission of **Hawking radiation** and the potential for **spontaneous excitation**, are expected to dominate. The accelerating reference frame of the black hole horizon introduces **thermal properties** that parallel the discussions of **thermal baths** in both high-energy accelerators and astrophysical objects.

transformation laws, and operations like symmetrization, antisymmetrization, and contraction. Tensors are mathematical objects that transform according to specific rules under a change of coordinates. A tensor of rank (k, l) has components $T_{\mu_1 \dots \mu_k \nu_1 \dots \nu_l}$, and these components transform in a particular way between different coordinate systems.

The rank of a tensor (k, l) describes its number of covariant (lower indices) and contravariant (upper indices) components. Common operations on tensors include:

1. **Symmetrization and Antisymmetrization:** These operations modify tensors by permuting their indices, with signs depending on the permutation's parity.
2. **Contraction:** This operation reduces the rank of a tensor by contracting (summing over) indices.
3. **Linear Transformation of Tensors:** A tensor transforms linearly under a change of basis in its vector space.

The document also includes mathematical tools like the **Kronecker delta** and the **Young tableau**, which classify tensors based on their symmetries and help calculate their dimensions. The process of

symmetrization and antisymmetrization, as well as contraction, plays an essential role in defining irreducible components of tensors.

```
# Tensor transformation law (Eq. 3.1.2)
T_prime = sum(x_alpha1, alpha1) * ... * x_alpha_l, alpha_l * x_nu1,
nu1 * ... * x_nu_k, nu_k * T

# Kronecker delta example (Eq. 3.1.3)
delta_mu_nu = x_alpha, alpha * x_beta, beta * delta_alpha_beta

# Symmetrization and Antisymmetrization (Eq. 3.1.4)
T_symmetric = (1 / p!) * sum(permuations(mu1,...,mu_p))
T_antisymmetric = (1 / p!) * sum((-1)^J *
permuations(mu1,...,mu_p))

# Contraction (Eq. 3.1.5)
T_contracted = sum(delta_alpha_beta * T_beta...alpha)

# Tensor transformation under coordinate change (Eq. 3.1.6)
P_prime = sum(x_gamma, gamma * x_delta, delta * x_alpha, alpha *
x_beta, beta * P)
Q_prime = sum(x_gamma, gamma * x_nu, nu * x_alpha, alpha * x_mu, mu *
Q)

# Young tableau example to calculate the dimension K of the linear
space (Eq. 3.1.12)
K = (D-2) * (D-1) * D^2 * (D+1)^2 * (D+2) * (D+3) / (6 * 4^2 * 3 *
2 * 1)
```

Elements of this space are called p-forms. In the space of forms two additional operations are defined: i) an exterior product (or wedge product) \wedge and ii) an exterior derivative. The wedge product $\gamma = \alpha \wedge \beta$ of a p-form α and of a q-form β is a (p+q) form that has the following components $\gamma_{\mu_1 \dots \mu_p \nu_1 \dots \nu_q} = (p+q)! p! q! \alpha_{\mu_1 \dots \mu_p} \beta_{\nu_1 \dots \nu_q}$.

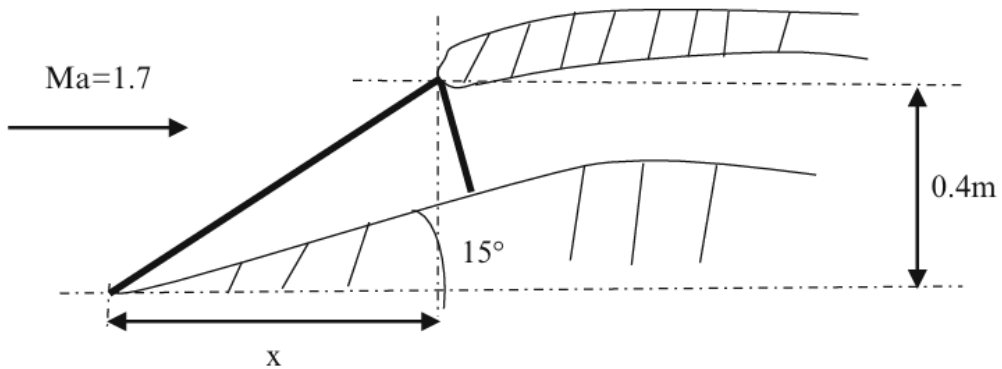
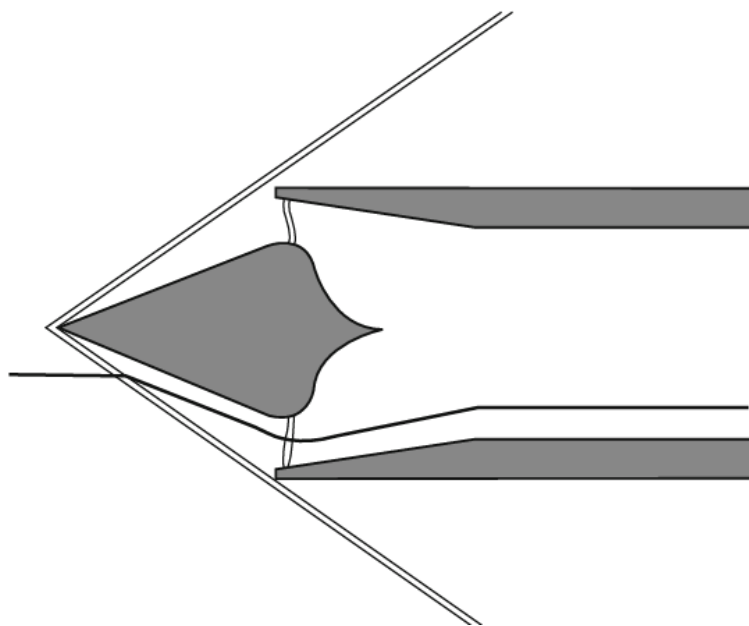
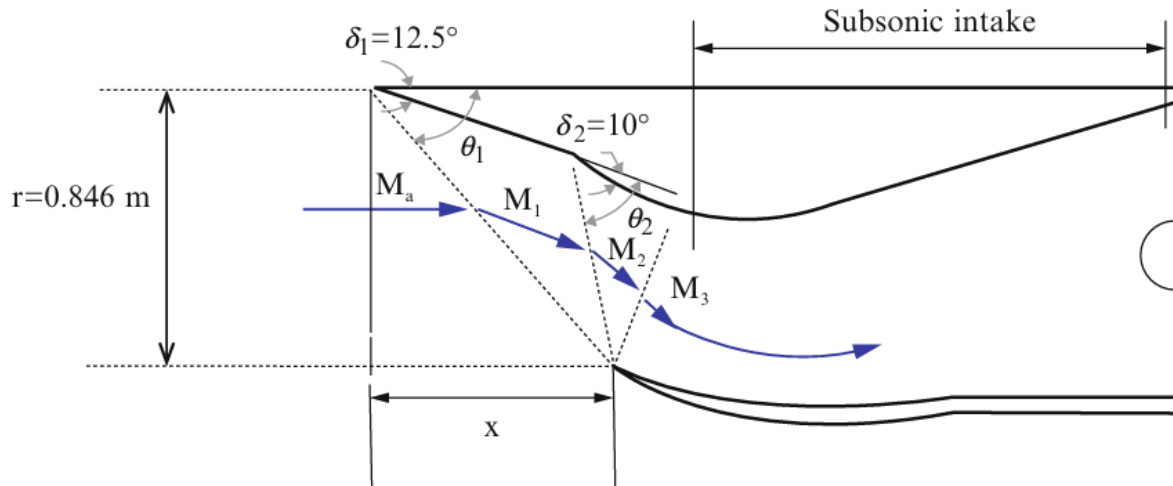


Figure: Problem (8.3)



Calculate the following:

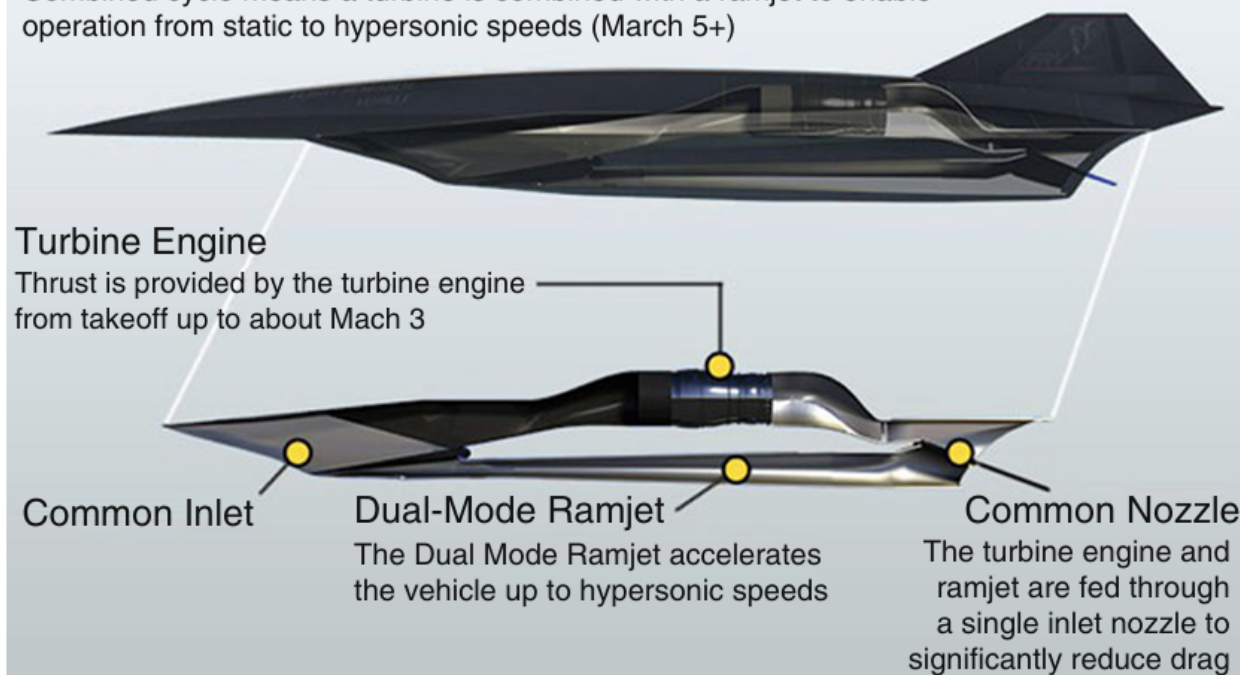
- (a) The Total pressure and temperature of air entering the first oblique shock wave
- (b) The first oblique shock wave angle (θ_1)
- (c) The pressure recovery along the first oblique shock
- (d) The Mach number after the first oblique shock wave
- (e) The second oblique shock wave angle (θ_2)
- (f) The Mach number after the second oblique shock wave
- (g) The pressure recovery along the second oblique shock
- (h) The Mach number after the normal shock wave
- (i) The pressure recovery along the normal shock wave
- (j) The total pressure recovery (where pressure recovery for subsonic intake ≈ 0.98)
- (k) The external distance of spike (X)



Isothermal reversible processes become isentropic in the limit of zero temperature. • It is impossible to reduce the temperature of any system to absolute zero in a finite number of operations. • A Stronger Version, proposed by Planck, states that: The entropy of any system tends, as $\rightarrow 0$, to an absolute constant, which may be taken as zero. Bardeen et al. (1973) formulated the analog of the third law for black holes in the following form: It is impossible by any procedure, no matter how idealized, to reduce the black hole temperature to zero in a finite sequence of operations. Since the black hole temperature vanish simultaneously with κ , this is only possible if an isolated stationary black hole is extremal: $M_2 = a_2 + Q_2$.

Turbine-Based Combined Cycle Propulsion

Combined cycle means a turbine is combined with a ramjet to enable operation from static to hypersonic speeds (March 5+)



b) Prove that the air-to-fuel ratio on a mass basis is:

$$28.97(1+12n+2n^2)3n(4.76) \text{ kg of air} / \text{kg of fuel} = \frac{28.97(1 + 12n + 2n^2)}{3n(4.76)} \text{ kg of air} / \text{kg of fuel}$$

c) Write down the combustion equation for the hydrocarbon fuels:



Combustion piece: “Afterburning” in a jet engine involves burning additional fuel in the: (A) Jet pipe (B) Turbine (C) Combustion chamber (D) Compressor

"exploring ways to combine the pieces of a black hole with additional components and dimensions that could be incorporated into a spacecraft engine or turbo propulsor. This also includes the theoretical possibility of gravitational manipulation with this new space object, incorporating Alcubierre drive and CTS (Curvature-Twisted Space).

Black hole piece: Let f be a diffeomorphism of a manifold M to N . If α is a chart in the vicinity of a point $p \in M$, then $\alpha \circ f^{-1}$ is a corresponding ('dragged along') chart in the vicinity of a point $p' = f(p) \in N$. A tensor T^* at p is said to be 'dragged along' by the map f ($T^* \equiv f^*T$) if its components in the corresponding 'dragged along' chart are the same as the components of the original tensor T at the initial point p in the original chart. If $f : M \rightarrow M$ is a diffeomorphism, and T is a tensor field on M , one can compare T with $T^* \equiv f^*T$. If $T = T^*$, then the tensor field is said to be invariant with respect to f .

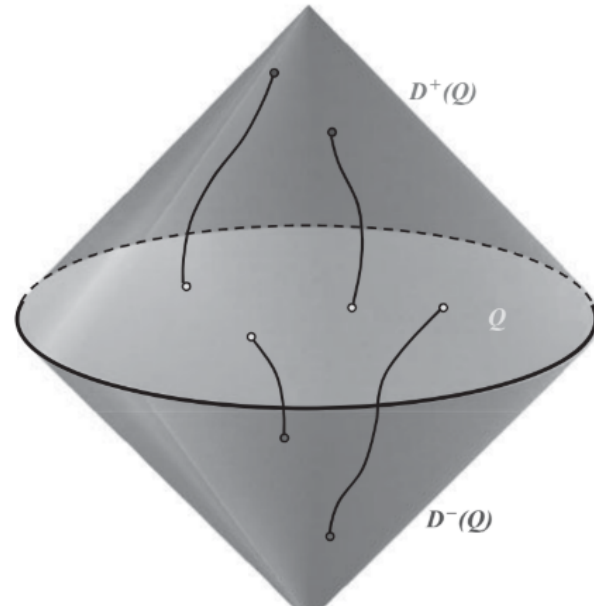


Fig. 3.6 Illustration of the future and past Cauchy domains for the set Q .

